Research Article | Vol. 26, No. 17 | 20 Aug 2018 | OPTICS EXPRESS 22457
Optics EXPRESS

Tailoring the mode-switching dynamics in quantum-dot micropillar lasers via time-delayed optical feedback

STEFFEN HOLZINGER,[1] CHRISTOPH REDLICH,[2] BENJAMIN LINGNAU,[2] MARCO SCHMIDT,[1] MARTIN VON HELVERSEN,[1] JÖRN BEYER,[3] CHRISTIAN SCHNEIDER,[4] MARTIN KAMP,[4] SVEN HÖFLING,[4,5] KATHY LÜDGE,[2] XAVIER PORTE,[1,*] AND STEPHAN REITZENSTEIN[1]

[1]*Institut für Festkörperphysik, Quantum Devices Group, Technische Universität Berlin, Hardenbergstraße 36, 10623 Berlin, Germany*
[2]*Institut für Theoretische Physik, AG Nichtlineare Laserdynamik, Technische Universität Berlin, Hardenbergstraße 36, 10623 Berlin, Germany*
[3]*Physikalisch-Technische Bundesanstalt, Abbestraße 2-12, 10587 Berlin, Germany*
[4]*Technische Physik, Universität Würzburg, Am Hubland, 97074 Würzburg, Germany*
[5]*SUPA, School of Physics and Astronomy, University of St Andrews, St Andrews, KY16 9SS, UK*
[*]*javier.porte@tu-berlin.de*

Abstract: Microlasers are ideal candidates to bring the fascinating variety of nonlinear complex dynamics found in delay-coupled systems to the realm of quantum optics. Particularly attractive is the possibility of tailoring the devices' emission properties via non-invasive delayed optical coupling. However, until now scarce research has been done in this direction. Here, we experimentally and theoretically investigate the effects of delayed optical feedback on the mode-switching dynamics of an electrically driven bimodal quantum-dot micropillar laser, characterizing its impact on the micropillar's output power, optical spectrum and photon statistics. Feedback is found to influence the switching dynamics and its characteristics time scales. In addition, stochastic switching is reduced with the subsequent impact on the microlaser photon statistics. Our results contribute to the comprehension of feedback-induced phenomena in micropillar lasers and pave the way towards the external control and tailoring of the properties of these key systems for the nanophotonics community.

1. Introduction

Quantum-dot (QD) micropillar lasers provide an attractive and versatile platform for investigating exciting physics at the crossroads between nanophotonics and nonlinear laser dynamics. In consequence, the extend of their physics and applications spread among both fields. From a nanophotonics viewpoint, coupled QD micropillar systems are excellent testbed devices for many key applications. Their small dimensions lead to pronounced light-matter-interaction in the regime of cavity quantum electrodynamics (cQED), where single-emitter effects and high spontaneous emission noise strongly influence the device functionality [1]. For QD micropillar systems, important cQED effects like strong photon-cavity coupling [2] as well as applications like optically and electrically triggered sources of single indistinguishable photons [3–5] and entangled-photon pairs [6] have been demonstrated. The transition to lasing is also affected in the regime of cQED. Particularly, lasing has been demonstrated in the single-QD regime [7] paving the way towards the limiting case of thresholdless lasing [8–12]. From the standpoint of nonlinear laser dynamics, high-β QD micropillar lasers show particular dynamical regimes not present in standard large-scale semiconductor lasers like partial injection locking [13]. Moreover, intrinsically nonlinear switching dynamics result from the gain-competition between the two

#328084 https://doi.org/10.1364/OE.26.022457
Journal © 2018 Received 10 Apr 2018; revised 20 Jul 2018; accepted 20 Jul 2018; published 17 Aug 2018

Optics EXPRESS

perpendicular polarizations of the micropillar fundamental mode [14]. Complex dynamics resulting from mode-competition have also been studied in other compact photonic systems like vertical-cavity surface-emitting lasers (VCSELs) [15] and photonic crystal nanolasers [16].

A well-known source of complex nonlinear dynamics in semiconductor lasers is delayed feedback and coupling [17, 18]. So far the nonlinear dynamics of feedback-coupled lasers have been mostly studied in the classical regime, where it presents a broad phenomenology and many related applications. Meanwhile the question of the limits of feedback effects when operating a laser with few photons in the cavity is still open. Recent theoretical predictions already illustrated the high impact that delayed optical feedback can have on the emission properties of cQED systems in the quantum regime [19, 20]. However, up to date only a limited number of experimental works have addressed the influence of delayed feedback on the behavior of QD micropillar lasers. Two early works [21, 22] addressed the basic phenomenology induced by delayed optical feedback. In a more recent publication [23] complex nonlinear dynamics have been reported in QD micropillar lasers subject to optoelectronic feedback in a monolithically integrated device concept. In the case of delayed optical feedback, the principal effects observed in the micropillars' emission were the change in photon statistics [21] and alteration of the mode intensities under polarized optical feedback [22]. The former effect consisted in super-thermal photon bunching of the central autocorrelation peak ($g^{(2)}(0) > 2$) that was interpreted as an indication of the feedback-induced chaotic dynamics.

Those early works already evidenced the strong impact that feedback can have in the photon statistics and in the interaction between the two micropillar emission modes. However, a proper understanding and control of the feedback effects is vital if we want to address fascinating applications such as random number generation [24], secure key exchange [25] and reservoir computing [26] with microlasers. Therefore, in our work we study in detail how delayed optical feedback affects the main emission properties of QD micropillar lasers. We observe that feedback unbalances the mode competition, modifying the position of the switching point in the microlaser input-output characteristics. Specifically around the crossing point, we observe enhanced mode-switching dynamics with the presence of multiple time scales that range from nanoseconds up to tenths of microseconds. A detailed study of the photon statistics denotes a drastic reduction of noise-related fluctuations all through the input-output, indicating a qualitative change in the nature of the dynamical bifurcation. Thus, we demonstrate that delayed optical feedback tailors the photon statistics and the mode switching of micropillar lasers, which are the two fundamental dynamical properties of such nanophotonic devices.

2. Devices under study

In our study we investigate electrically driven micropillar lasers using a single layer of $In_{0.3}Ga_{0.7}As$ quantum dots with an area density of $5 \cdot 10^9/cm^2$ acting as a gain medium in the center of a one-λ GaAs cavity. The planar microcavity is formed by a lower and an upper distributed Bragg reflectors (DBR) with 27 and 23 AlAs/GaAs mirror pairs, respectively. The pillar structures with a diameter of 4 μm are fabricated using high-resolution electron-beam lithography and plasma etching. After planarizing the sample with dielectric benzocyclobutene, 120 pillars can be simultaneously pumped via ring-shaped gold contacts that converge in one bar. The quality (Q) factor of the investigated micropillar can be estimated from the linewidth measured at inversion to be $Q \simeq 20000$. Because of a slight structural asymmetry, the degeneracy of the two orthogonally polarized modes of the micropillar (from now on called strong and weak mode) is lifted resulting in the characteristic bimodal emission with a mode splitting of 117 μeV [27]. For further details on sample fabrication we refer to Ref. [28].

To study the emission properties of our QD micropillar lasers, we apply a setup equipped for measuring spectroscopic features as well as quantum optic signatures of the emission statistics. The latter being indispensable when aiming to unambiguously prove lasing emission from high-β

Optics EXPRESS

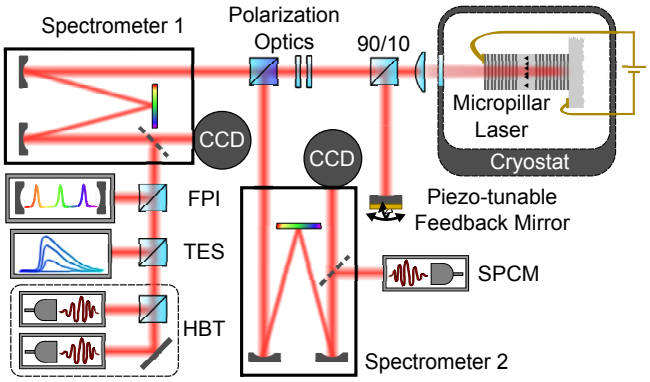

Fig. 1. Sketch of the micro-photoluminescence (μPL) setup used for our measurements. The micropillar is kept at cryogenic temperatures (T ~ 5 – 40 K) inside a He-flow cryostat. The spectral properties are measured with a grating spectrometer equipped with a CCD camera, or alternatively with a high-resolution Fabry-Perot interferometer (FPI). The dynamical signatures and the photon statistics are characterized via single-photon counting modules (SPCMs) (in different configurations depending on the measurement) and via a photon-number resolving transition-edge sensor (TES) detector.

devices [12, 29, 30], or when addressing the problem of measuring dynamics in nW-output power devices [21]. The experimental setup is schematically depicted in Fig. 1. The sample is mounted in a continuous flow He-cryostat and its temperature is set to T = 32.00 ± 0.01 K. Electrical excitation is provided by a precision DC-voltage source. An aspherical lens (NA = 0.5) collects the micropillar emission, which is then spatially filtered by a pinhole and analyzed with a spectrometer (spectral resolution ≈ 6.5 GHz) or alternatively with a scanning Fabry-Perot interferometer (7.5 GHz free spectral range, 100 MHz resolution) for higher spectral resolution. The second-order autocorrelation function ($g^{(2)}(\tau)$) can be obtained by using two fiber-coupled Si-based single-photon counting modules (SPCMs) in combination with time-correlation electronics forming a Hanbury-Brown and Twiss interferometric setup [31]. The emission is going through the spectrometer (with spectral window of 0.1 nm centered at 900 nm in the given configuration) to spectrally filter the emission from the wetting layer, which would otherwise add a significant amount of uncorrelated background signal to the photon statistics. The polarization is independently selected by using specific polarization optics (half-wave plate in combination with a polarizing beam splitter) as indicated in Fig. 1. Our external cavity consists of a 90/10 beam splitter (90% reflection) and a mirror. The delay time of such cavity is τ_{FB} = 5.9 ns. We want to note that the alignment of the feedback spot to the micrometer-scale upper facet of the micropillar is a particularly sensitive point of our experiment which requires high mechanical stability and fine-tuning capabilities. For that reason we use a piezo-tunable mirror, that gives us a precision in the position of the feedback spot of ≃ 0.4 μm. For alignment we choose a current where the strong mode shows a significant decrease in output intensity when feedback is applied. Optimal feedback coupling is found when the minimum intensity is reached when scanning the feedback spot on the upper facet of the microlaser with the piezo mirror (25x25 X-Y-steps with step size of approximately 0.4 μm), making this routine fully reproducible.

In order to experimentally measure the very informative photon-number distribution, a transition-edge sensor (TES) detector was used as a highly sensitive calorimeter. The TES is voltage-biased to the operation point of the phase transition region between superconducting and normal conducting (~ 150 mK). Thus, a TES is able to detect the amount of energy dissipated

Optics EXPRESS

from photon absorption with the resolution of a single photon [32]. The induced temperature increase results in a change of current which can be measured by an inductively coupled two-stage dc-superconducting quantum interference devices (SQUID / current sensor) [33]. Because of the long thermal recovery time of the detector after photon detection ($\sim 1\,\mu s$) the TES cannot be used in continuous wave detection mode. Therefore, an electro-optical modulator (EOM) is placed in the detection path generating transmission windows of 15 ns duration at a repetition rate of 1 kHz. Data recording at the TES output signal is synchronized to the EOM pulse sequence, so it is also possible to identify zero-photon events. We carefully selected the gating time-window so that we could measure photon numbers clearly larger than 1 and, simultaneously, we could differentiate between different dynamical regimes. Moreover, since the rise and fall times of the optical pulses are very short compared to the pulse length, they do not affect the measured photon number distributions.

The histogram of the photon-number distribution is then extracted from 50000 trigger events with a detection efficiency of 87 % [34].

3. Numerical simulations

We theoretically describe the delayed feedback laser within the semiclassical four-variable rate-equation model that was successfully used in [14]. Additionally, a quantum Langevin approach allows us to investigate the microlaser system in the cQED weak coupling regime. Hence we work with a stochastic delay differential equation system (SDDE) for the bimodal complex electric fields $E_{s,w}$ (strong and weak modes respectively), the occupation probability ρ of the active quantum dots and the reservoir carrier density n_r. Delayed optical feedback is included in the differential equations by adding $-K_j E_j(t-\tau_{FB})$.

$$\frac{\mathrm{d}}{\mathrm{d}t}E_j(t) = \tfrac{1}{2}\tfrac{h\nu_0}{\epsilon_0\epsilon_{bg}}\tfrac{2Z^{QD}}{V} g_j\,(1+i\alpha)\left[2\rho(t)-1\right]E_j(t) - \kappa_j\left(E_j(t) - K_j E_j(t-\tau_{FB})\right) + \sqrt{\tfrac{h\nu_0}{\epsilon_0\epsilon_{bg}}\tfrac{2Z^{QD}}{V}\beta\tfrac{\rho}{\tau_{sp}}}\xi(t) \tag{1}$$

$$\frac{\mathrm{d}}{\mathrm{d}t}\rho(t) = -\sum_{j\in\{sw\}} g_j\left[2\rho(t)-1\right]|E_j(t)|^2 - \frac{\rho(t)}{\tau_{sp}} + S^{in}n_r(t)\left[1-\rho(t)\right] \tag{2}$$

$$\frac{\mathrm{d}}{\mathrm{d}t}n_r(t) = \tfrac{\eta}{e_0 A}(I-I_p) - S^{in}n_r(t)\tfrac{2}{A}Z^{QD}\left[1-\rho(t)\right] - S^{in}\tfrac{2}{A}Z^{inac}\frac{\rho^{inac}}{\tau_{sp}} - \frac{n_r(t)}{\tau_r} \tag{3}$$

$$\text{with } g_j = \tfrac{|\mu_j|^2 T_2}{2\hbar^2}\left(1+\varepsilon_{js}\tilde{\varepsilon}|E_s(t)|^2 + \varepsilon_{jw}\tilde{\varepsilon}|E_w(t)|^2\right)^{-1} \tag{4}$$

The electric field optical losses $\kappa_{s,w}$ are given by the experimental cavity quality factor $Q_{s,w}$ using $\kappa_{s,w} = (\pi\nu_0)/Q_{s,w}$ with ν_0 being the center frequency of the free running laser line that is determined from the experiment to be $\nu_0 \simeq 334$ THz (1.38 eV). A quality factor of $Q \approx 20000$ leads to losses $\kappa_s = 52\,\mathrm{ns}^{-1}$ and $\kappa_w = 54.7\,\mathrm{ns}^{-1}$. A phenomenological linewidth enhancement factor with a value of $\alpha = 1.0$ is included in the equations of both electric field modes.

In contrast to conventional lasers with large mode volumes, the low mode-volume microlaser with $V = 4\,\mu\mathrm{m}^3$ shows cQED enhanced light-matter coupling that is captured using stochastic spontaneous emission noise with a Purcell-shortened spontaneous emission lifetime within one QD of $\tau_{sp} = 0.23$ ns (compared to about a typical QD lifetime of about 1 ns in bulk) and spontaneous coupling factor $\beta = \frac{r_{laser}}{r_{sp}} = 1.8\,\%$. The value of β is extracted from the fit of the experimental input-output curve, see Fig. 2. We model the mode interaction by means of gain compression of the form $g_j \sim \left(1+\varepsilon_{js}\tilde{\varepsilon}|E_s|^2 + \varepsilon_{jw}\tilde{\varepsilon}|E_w|^2\right)^{-1}$. The gain-compression factors are set accordingly to yield very good quantitative agreement with the experimental data (cf. Table 1).

Optics EXPRESS

Those factors significantly determine the interplay of weak and strong modes and are crucial to shape the two mode emission characteristics. In particular, the cross-compression factors give rise to a bistability between the emissions of weak and strong modes. Hence, both modes are coupled via the common gain medium of active QDs, giving rise to a variety of dynamical scenarios that include fast mode switching, uni- or bistable single-mode emission as well as bimodal emission. The inversion $(2\rho - 1)$ is determined by losses from the induced emission process, proportional to $\sum_j g_j(2\rho - 1)|E_j|^2$, spontaneous emission losses $\frac{\rho}{\tau_{sp}}$ and effective in-scattering $S^{\text{in}}\, n_r\, (1-\rho)$ from the effective reservoir carrier density n_r, where we account for Pauli-blocking using the term $(1-\rho)$. The effective in-scattering rate $S^{in} = 0.007\,\frac{\text{m}^2}{\text{ns}}$ is extracted from measurements of the relaxation oscillations of the microlaser under small-amplitude short optical perturbations.

Table 1. Table of additional parameters used for the simulations if not stated otherwise in the main text.

Parameter		Value
Dipole transition moment strong (weak) mode	μ_s (μ_w)	2.50 (2.42) nm×e_0
Effective dephasing time	T_2	0.33 ps
Background refractive index	n_{bg}	3.34
-	$\tilde{\varepsilon}$	$\varepsilon_0 n_{bg} c_0$
Auto-compression factors	ε_{ss}	$29\times10^{-10}\,\frac{m^2}{AV}$
-	ε_{ww}	$24\times10^{-10}\,\frac{m^2}{AV}$
Cross-compression factors	ε_{ws}	$31\times10^{-10}\,\frac{m^2}{AV}$
-	ε_{sw}	$42\times10^{-10}\,\frac{m^2}{AV}$

In agreement with the typical densities of QDs in such materials of $n_{QD} = 5\times10^9\text{cm}^{-2}$ and the given spatial and spectral overlap with the fundamental cavity mode, we consider $Z^{QD} = 250$ QDs (out of a total of 650 QDs in the active layer) contributing actively to the emission of the micropillar with a mode area of $A \approx 3.1\,\mu\text{m}^2$ [35]. The $Z^{inac} = 400$ "inactive" dots are not resonant to the cavity mode, but still capture carriers from the reservoir. The carrier reservoir is pumped by the electrical current I. A pump efficiency $\eta = 9.4\%$ and a parasitic current $I_p = 2.7\,\mu\text{A}$ are included in the model, to take care of the fact that the 120 microlasers are coupled via a common current bar of the electrically pumped sample. Reservoir losses are included with a decay term $-n_r/\tau_r$, where the carrier life time τ_r is set to 1 ns. Table 1 gives a list of the additional parameters, that are not mentioned in the text.

4. Tailoring the microlaser properties with delayed optical feedback

In this section, we present the effects of delayed optical feedback on the basic optical characteristics of our QD micropillar lasers. These microlasers maintain lasing with the gain of a low number of quantum dots resulting in a few hundreds of photons in the cavity with sub-μW output power [12, 36]. Because of its small diameter (≃ 4 μm) and the optimized spectral matching of the QD ensemble emission, the investigated micropillar only exhibits lasing on the fundamental Gaussian mode. Transverse modes of higher order appear strongly suppressed and can be disregarded. As the azimuthal order of the fundamental mode is zero it can oscillate in two different states of polarization as observed in VCSELs [37,38]. The lifted mode energy degeneracy

Optics EXPRESS

above the lasing threshold results in a competition for the common gain leading to switching dynamics between those modes.

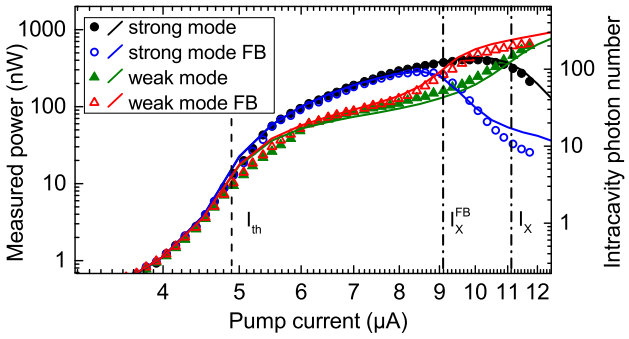

Fig. 2. Input-output characteristics of the micropillar laser with and without feedback (FB). Experimentally measured data points are indicated by symbols whereas numerical simulations are shown as solid lines. The lasing threshold current (I_{th}) is indicated by a dashed line and the intensity crossing points without and with FB (I_x and I_x^{FB} respectively) are indicated by dashed-dotted lines.

Figure 2 shows the input-output characteristics of the investigated microlaser. The optical spectra of the micropillar are fitted with a Gaussian and the resulting area of the Gaussian fit is then compared with a direct measurement of the optical output with a powermeter. Using this calibration method we can relate the optical spectra with an output power in nW.

While the strong mode shows the typical shallow s-shape transition to lasing of a high-β laser, the weak mode increases much less at threshold. Only at higher excitation strength the weak mode shows an increase (accompanied with a saturation and decrease of the strong mode) leading to a crossing of the modes intensities at the current $I_x = 11.2$ μA. This behavior is typical when driving microlasers with increasing current above lasing threshold as an effective spectral shift of the gain also changes its overlap with respect to each mode. The measured input-output characteristics are accurately reproduced by our numerical model in quantitative agreement which allows us to precisely set the respective parameters of our model. According to the simulations, the onset of stimulated emission occurs at a current of $I_{th} = 4.9$ μA. Here the average photon number in the cavity is approximately 7, which is consistent with values of $\sim \beta^{-1/2}$ predicted by theory [39]. The intracavity photon number is then calculated from the output power based on the power at threshold. The investigated laser shows a rather smooth transition from spontaneous to stimulated emission. This behavior is typical for cQED enhanced microlasers [40] and stands in contrast with conventional lasers with β typically $\sim 10^{-5}$, where the emission intensity and linewidth experience drastic changes above threshold. In the current region close to the intensities crossing point, spontaneous emission noise enhances the switching between the two orthogonally polarized modes. For a detailed bifurcation analysis of this scenario we refer to [14], in which the underlying bistability causing intense multiphoton pulsations is studied.

In the previous studies on feedback-coupled micropillar lasers [21, 22], optical feedback had little effect on the average output intensity of the modes. This observation is explained by the fact that the input-output characteristics was strongly dominated by one mode. In contrast, here we go well beyond previous studies by exploring the rich dynamics of a bimodal micropillar laser with two similar modes whose input-output curves remain close and eventually cross. When applying feedback, the intensity of both modes decreases and the crossing point is shifted to

Optics EXPRESS

a lower excitation current ($I_x^{FB} = 9.1\,\mu A$). Our external cavity roundtrip time ($\tau_{FB} = 5.9\,ns$) is greater than the coherence time of the laser and allows us to study the regime of incoherent feedback. Analog to previous studies, no pronounced change in threshold current as well as no hysteresis of output intensity between the increase and decrease of the excitation current can be observed. These effects are masked by the high spontaneous emission noise which smooths out the gain clamping at laser threshold [13].

Correlation and spectral properties

The low output intensities of micropillar lasers, well below 1 μW, prevent from the direct experimental measurements of temporally resolved time traces. Therefore, the second-order autocorrelation function $g^{(2)}(\tau)$ becomes a fundamental measurement to understand the microlaser dynamics because unstable or pulsing behavior in each mode of our QD micropillar is directly reflected in a deviation from the constant $g^{(2)}(\tau) = 1$ of a perfect Poissonian laser source. We consequently characterize in detail $g^{(2)}(\tau)$ and the correlation times (τ_{corr}) with respect to the pump current. Figure 3(a) shows $g^{(2)}(\tau = 0)$ for both the strong mode and weak mode. The strong mode experiences a smooth transition from thermal $g^{(2)}(0) = 2$ to coherent emission $g^{(2)}(0) = 1$, as expected for high-β lasers. For excitation currents below lasing threshold, the thermal bunching cannot be resolved because of insufficient temporal resolution of the SPCMs (57 ps). The weak mode does not undergo a complete transition to lasing due to the multi-photon pulse behavior [14] for pump currents below (I_x), as indicated by $g^{(2)}(0) > 1$ in this current range. Around that point, we can also observe that $g^{(2)}(0)$ correctly reflects the change of character between both modes, i.e., the strong mode becomes super-thermal (increase of $g^{(2)}(0)$) while the weak mode changes to laser-like values ($g^{(2)}(0) \rightarrow 1$). In Figs. 3(b) and 3(c), the correlation time τ_{corr} extracted from the decay of $g^{(2)}(\tau)$ is shown with symbols and compared with the coherence time τ_{coh} as extracted from the linewidth of experimental optical spectra (dashed curves). In contrast to the variable behavior of $g^{(2)}(0)$, the measured correlation times monotonously increase, even around the switching point. Furthermore, τ_{corr} diverges more significantly from τ_{coh} in the region of super-thermal bunching of $g^{(2)}(0)$, indicating that the correlation time reflects the switching timescales.

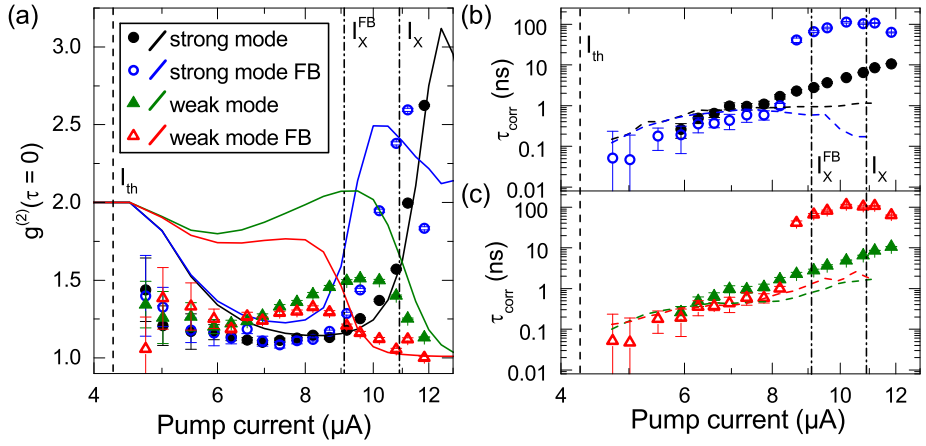

Fig. 3. Measured and simulated pump dependence of the second-order autocorrelation function (a) and correlation time scales (b,c). For comparison with τ_{corr}, we show in panels (b) and (c) the measured coherence times τ_{coh} (colored dashed lines). The vertical dotted and dash-dotted lines indicate the threshold and intensity crossing currents respectively [Fig. 2].

Optics EXPRESS

Optical feedback leads to significant changes in $g^{(2)}(\tau)$ and τ_{corr}. As already seen in the input-output characteristics, feedback shifts the crossing point I_x to lower pump currents and the strong mode undergoes super-thermal bunching at lower excitation currents. Moreover, these intensity crossing points are coinciding with the crossing points of $g^{(2)}(0)$ proving a shift of the dynamical regimes towards lower pump currents by feedback. For both modes, until the injection current approaches I_x^{FB}, the correlation times are lower than in the no-feedback scenario [Figs. 3(b) and 3(c)]. This indicates that delayed optical feedback suppresses the noise-induced switching dynamics for low-to-intermediate excitation currents. At the crossing point of the intensity of both modes the correlation time increases by about two orders of magnitude which can be related to switching with much longer dwelling times.

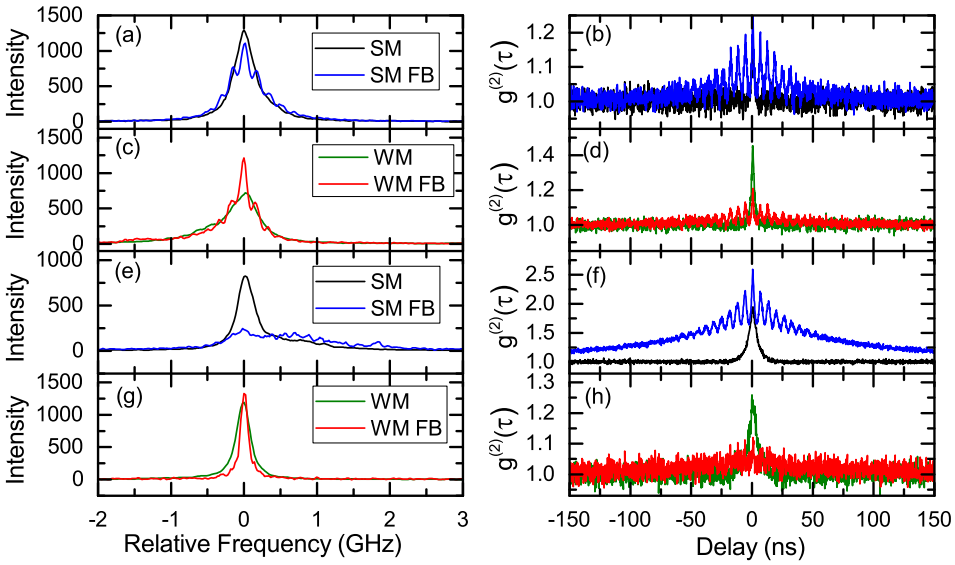

Fig. 4. Measured optical spectra (left panels) and corresponding $g^{(2)}(\tau)$ (right panels) for both solitary and feedback scenarios. The optical spectra have been recorded using the FPI with 75 MHz frequency resolution. The pump current condition is I_x^{FB} for panels (a)-(d) and I_x for panels (e)-(h).

To understand better the interrelation between the micropillar dynamics and time scales, we compare the complete information stored in $g^{(2)}(\tau)$ with the corresponding optical spectrum. Figure 4 depicts both measurements together for the pump currents of the intensity crossing points, I_x and I_x^{FB}. Figures 4(a) and 4(c) depict the effect of optical feedback on the optical spectrum at I_x^{FB}. The characteristics in absence of feedback are always depicted in order to compare both scenarios. We observe that under optical feedback the optical spectrum is modulated with the external cavity modes (ECM). Those modes are spaced with a frequency of 169 MHz corresponding to the inverse of the delay time $\tau_{FB} = 5.9$ ns, which is the time scale present between the revival peaks in the corresponding $g^{(2)}(\tau)$ [Figs. 4(b) and 4(d)]. The delay time τ_{FB} coexists in our system with two additional time scales, the fast decay of the individual revival peaks (τ_{coh}) and the slow decay of the envelope (τ_{corr}). The difference between these two latter time scales becomes extreme when we increase the injection current to I_x, as shown in Fig. 4(f). Here we observe that the strong mode shows super-thermal bunching above $g^{(2)}(0) = 2.5$ accompanied with a τ_{corr} that extends far beyond 100 ns. We interpret this very slow decay as the result of the mixing of multiple time scales in the dynamics, which would be confirmed by observation of the optical spectrum in Fig. 4(e). Here the linewidth of the micropillar laser

Optics EXPRESS

experiences a total collapse, the external cavity modes are no longer visible and the optical line broadens to the multi-GHz range. Noteworthy, for the same pump condition the weak mode depicts coherent spectral properties with $g^{(2)}(\tau) \rightarrow 1$ reflecting the significantly different behaviors coexisting in this micropillar laser.

At this point, it is interesting to explicitly measure the possible correlations between both micropillar modes dynamics. To do that, we experimentally measure the bimodal cross-correlation ($g^{(2)}_{SM-WM}(\tau)$) using a polarizing beam splitter to split the optical paths of both modes. Each mode goes then to a different monochromator and its intensity is measured with a SPCM. The second-order cross-correlation function is then calculated with a time-to-digital converter. Figure 5(a) shows clear anticorrelation behavior with increasing excitation current. The measurement of $g^{(2)}_{SM-WM}(\tau = 0) < 1$ proves that both modes exhibit anti-correlated dynamics. Minimal values of $g^{(2)}_{SM-WM}$ are obtained at the intensity crossing point I_x of the two modes both with and without feedback. The addition of feedback, again leads to a strong increase of the characteristic correlation times together with a periodic pattern of minima at multiples of the delay time. Figure 5(b) depicts the experimentally and numerically extracted values of $g^{(2)}_{SM-WM}(\tau = 0)$. We can observe that $g^{(2)}_{SM-WM}(0)$ has its minimum at the intensity crossing point of both modes, which is consistent with the case without feedback. This behavior is also confirmed by numerical simulations (solid lines) that are in good qualitative agreement with experimental data. The fact that the experimental values of the crosscorrelation function are slightly higher than in theory is caused by the use of a polarizing beam splitter with finite splitting ratio that does not provide perfect polarization suppression of the counterpart mode. Interestingly, for high-enough excitation currents, feedback stabilizes weak mode lasing, destroying the anti-correlated dynamics as was already indicated by the weak mode winning the gain competition [Fig. 2] and the behavior of the autocorrelation function $g^{(2)}_{SM} >> 1$ while $g^{(2)}_{WM} \sim 1$ [Fig. 3(a)]. This result shows that the mode-switching dynamics of a micropillar laser can be controlled via delayed optical feedback.

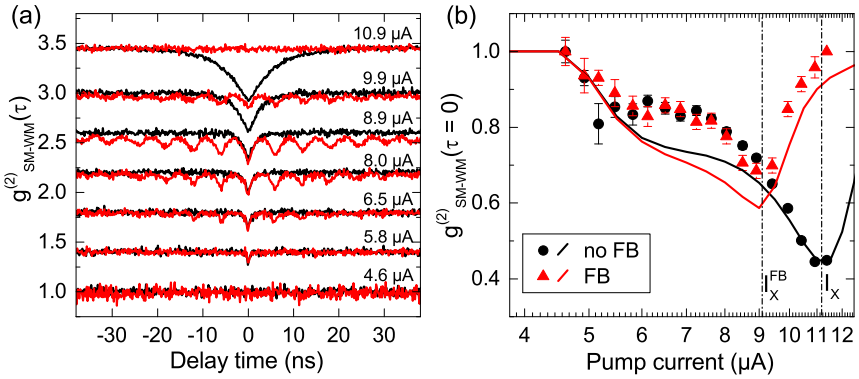

Fig. 5. Cross-correlation of strong and weak modes $g^{(2)}_{SM-WM}(\tau)$. Panel (a) depicts the measured $g^{(2)}_{SM-WM}$ for different pump currents without feedback (black) and with feedback (red). Panel (b) shows measured and simulated data for $g^{(2)}_{SM-WM}$ at $\tau = 0$ as a function of the pump current. Numerical simulations and experimental data are plotted in solid lines and points respectively.

Photon statistics

In analogy to the direct mode-switching measurement, an explicit measure of the photon statistics will provide a more complete picture of the statistical nature of the micropillar emission under

Optics EXPRESS

optical feedback. Our numerical simulations include a stochastic noise term. Thus, a statistic distribution of the laser output for a given pump current is obtained by calculating an ensemble of different noise realizations.

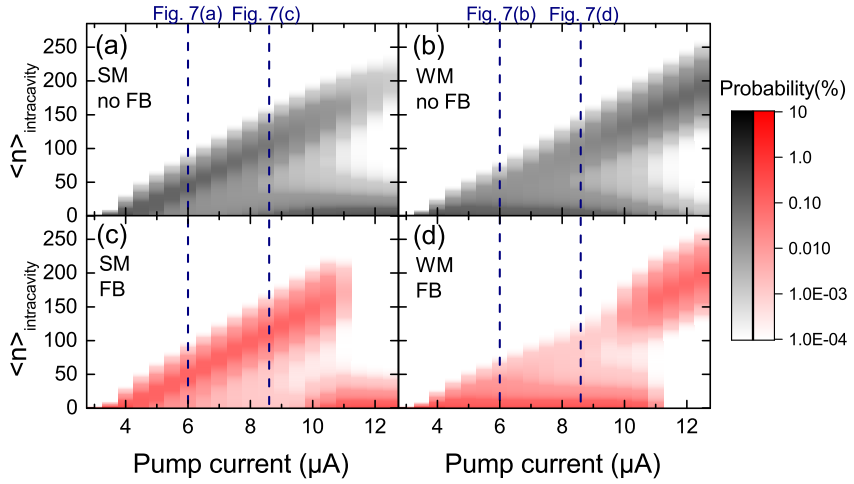

Fig. 6. Statistics and bistability of the input-output characteristics. Panels (a) and (c) are depicting the strong mode without and with feedback, respectively, while (b) and (d) show the emission of the weak mode. Vertical blue dashed lines indicate the currents where the photon-number distribution is measured with the TES detector [Fig. 7].

Figure 6 depicts the numerically obtained statistics of 50000 runs for increasing pump currents. They are plotted as heat maps where the scale encodes the probability to detect a certain intracavity photon number. Figures 6(a) and 6(b) present both modes without feedback. Above threshold, first the strong mode turns on and exhibits stable emission. Increasing pump current the micropillar enters an intermediate region of bimodal statistics between $\sim 8-11$ μA. A further increase of pump current finally leads to changing roles between strong and weak modes which was also evident from the total intensity. Applying optical feedback [Figs. 6(c) and 6(d)] stabilizes the individual modes. Moreover, the intermediate region becomes less prominent leading to a more abrupt change of roles at the intensity crossing point $I_x = 11.2$ μA. We conclude that delayed optical feedback reduces the stochastic switching between both micropillar modes, as already suggested in Fig. 5, pinning the less frequent switching events to the delay time. This can be understood from the perspective of stochastic systems. In such systems time-delayed feedback is known to stabilize oscillations and switching events by reintroducing the fluctuations as a driving term after the feedback time. This in turn generally leads to an increase of the correlation times with increasing feedback strength and delay (see, e.g., [41]).

Vertical slices through Fig. 6 yield the photon number distribution which can also be directly measured. Figure 7 depicts the comparison between theoretical curves and the experimentally measured photon number distribution for two selected pump currents (marked in blue dashed lines in Fig. 6). Bar histograms refer to the probability of the measured photon number (bottom axis) by the transition edge sensor (TES) detector, while solid lines are the vertical slices of the numerical data. The latter is providing the intracavity photon number (top axis) while the measured photon number which is expected to be on the order of 10^4 in the 15 ns gate is reduced due to losses in the detection path and detector efficiency. We want to point out that despite the attenuation of the signal by approximately 3 orders of magnitude we can still access the

Optics EXPRESS

underlying photon statistics as it is discussed in a recent publication [42].

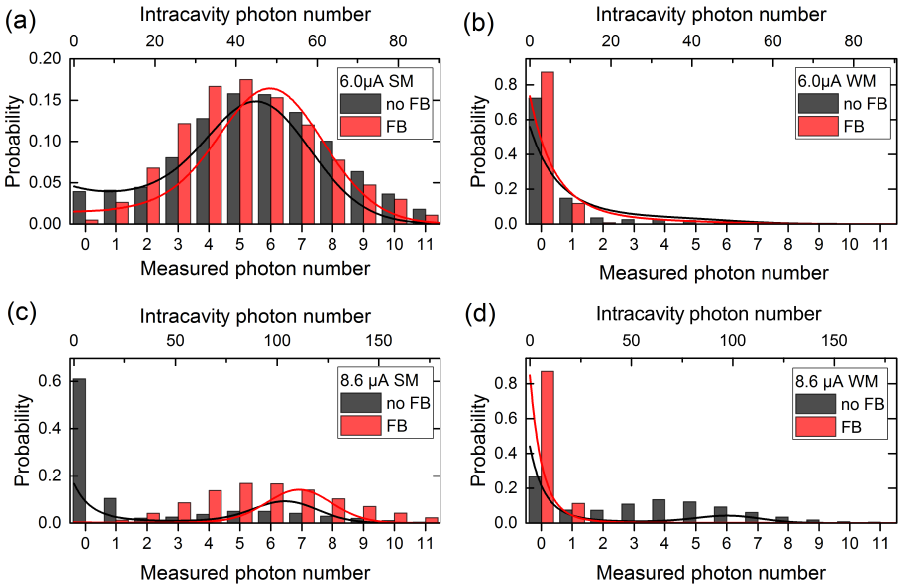

Fig. 7. Photon statistics. Bars in the histogram represent experimental data recorded with the TES, while solid lines are vertical slices of the simulated stochastic data shown in Fig. 6. The latter are referenced with the top axis representing the intracavity photon number and are rescaled for better comparison. Panels (a) and (b) depict the photon-number distribution for $I = 6.0\,\mu$A for the strong mode (a) and for the weak mode (b), respectively. Same for panels (c) and (d) but for a higher pump of $I = 8.6\,\mu$A.

Figure 7(a) clearly reveals the Poissonian statistics of the strong mode with a thermal tail (indicated by significant events for $n = 0$). Optical feedback strongly suppresses this thermal emission tail, effectively increasing the strong mode coherence. The photon distribution of the weak mode depicted in panel (b) resembles that of a thermal emitter. Only the multiple events at high photon numbers ($n > 3$) deviate from the expected thermal distribution, indicating that this mode already experiences switching events at the selected current. Here, feedback acts in the opposite direction than for the strong mode, reducing the probability of higher photon number events and making the photon statistics more thermal. Panels (c) and (d) depict respectively the strong and weak modes for a higher pump current of 8.6 μA. Both modes exhibit now clear superposition of Poissonian and thermal statistics. Nevertheless, we observe again how feedback strongly affects the bimodal behavior, stabilizing lasing and thermal emissions for the strong and weak modes, respectively. Those results show that delayed optical feedback can tailor the photon statistics of bimodal micropillar lasers by stabilizing their inherent stochastic switching dynamics.

5. Conclusions

In this work we have studied the effects of delayed optical feedback on high-β quantum-dot microlasers operating in the regime of cQED. The two orthogonally polarized components supported by the fundamental mode compete for the common QD gain leading to bistable switching dynamics and to a complex input-output dependence where the two modes cross with respect to their intensities and exchange their emission roles. When applying optical feedback we find a reduction of excitation needed to reach that crossing point. We analyze the change of the photon statistics for two operation currents representative of different dynamical regimes.

Optics EXPRESS

The two modes bistability is strongly influenced in both cases and can even be destroyed, so that stability in the emission of both modes is enhanced. This result can be advantageous for combined schemes with optical injection that has been predicted to strongly enhance the modulation properties of nanolasers [43]. From photon statistics measurements, we find that the system undergoes a transition towards mixed states through the input-output, which again can be tailored by optical feedback.

Despite the stabilization of the switching, the mode with lower output intensity shows highly unstable complex dynamics with strong feedback signatures in the second-order autocorrelation and the optical spectrum. This finding is significant for potential use of microlasers in nonlinear dynamics applications. In particular, the periodicity with delay time found in $g^{(2)}_{SM-WM}(\tau)$ hints at interesting anti-correlated complex dynamics that could be used for all-optical flip-flop memories [44].

The presented findings pave the way for understanding and tailoring the nonlinear dynamics and the photon statistics of high-β microlasers, representing a milestone towards external control of nanophotonic quantum systems.

Funding

European Research Council under the European Union's Seventh Framework Program (ERC Grant Agreement No. 615613); German Research Foundation (CRC 787, GRK1558); project EMPIR 14IND05 MIQC^2 co-financed by the Participating States and from the European Union's Horizon 2020 research and innovation program.

Acknowledgments

We thank A.E. Lita and S.W. Nam for providing the TES detector chips.

References

1. S. Reitzenstein and A. Forchel, "Quantum dot micropillars," J. Phys. D: Appl. Phys. **43**, 033001 (2010).
2. J. P. Reithmaier, G. Sek, A. Löffler, C. Hofmann, S. Kuhn, S. Reitzenstein, L. V. Keldysh, V. D. Kulakovskii, T. L. Reinecke, and A. Forchel, "Strong coupling in a single quantum dot-semiconductor microcavity system." Nature **432**, 197 (2004).
3. C. Santori, D. Fattal, J. Vučković, G. S. Solomon, and Y. Yamamoto, "Indistinguishable photons from a single-photon device," Nature **419**, 594 (2002).
4. S. Ates, S. M. Ulrich, S. Reitzenstein, A. Löffler, A. Forchel, and P. Michler, "Post-selected indistinguishable photons from the resonance fluorescence of a single quantum dot in a microcavity," Phys. Rev. Lett. **103**, 167402 (2009).
5. A. Schlehahn, A. Thoma, P. Munnelly, M. Kamp, S. Höfling, T. Heindel, C. Schneider, and S. Reitzenstein, "An electrically driven cavity-enhanced source of indistinguishable photons with 61% overall efficiency," APL Photon. **1**, 011301 (2016).
6. A. Dousse, J. Suffczyński, A. Beveratos, O. Krebs, A. Lemaître, I. Sagnes, J. Bloch, P. Voisin, and P. Senellart, "Ultrabright source of entangled photon pairs," Nature **466**, 217 (2010).
7. C. Gies, F. Gericke, P. Gartner, S. Holzinger, C. Hopfmann, T. Heindel, J. Wolters, C. Schneider, M. Florian, F. Jahnke, S. Höfling, M. Kamp, and S. Reitzenstein, "Strong light-matter coupling in the presence of lasing," Phys. Rev. A **96**, 023806 (2017).
8. M. Khajavikhan, A. Simic, M. Katz, J. H. Lee, B. Slutsky, A. Mizrahi, V. Lomakin, and Y. Fainman, "Thresholdless nanoscale coaxial lasers," Nature **482**, 204 (2012).
9. I. Prieto, J. M. Llorens, L. E. Muñoz-Camúñez, A. G. Taboada, J. Canet-Ferrer, J. M. Ripalda, C. Robles, G. Muñoz-Matutano, J. P. Martínez-Pastor, and P. A. Postigo, "Near thresholdless laser operation at room temperature," Optica **2**, 66 (2015).
10. M. Takiguchi, H. Taniyama, H. Sumikura, M. D. Birowosuto, E. Kuramochi, A. Shinya, T. Sato, K. Takeda, S. Matsuo, and M. Notomi, "Systematic study of thresholdless oscillation in high-β buried multiple-quantum-well photonic crystal nanocavity lasers," Opt. Express **24**, 3441 (2016).
11. Y. Ota, M. Kakuda, K. Watanabe, S. Iwamoto, and Y. Arakawa, "Thresholdless quantum dot nanolaser," Opt. Express **25**, 19981 (2017).
12. S. Kreinberg, W. W. Chow, J. Wolters, C. Schneider, C. Gies, F. Jahnke, S. Höfling, M. Kamp, and S. Reitzenstein, "Emission from quantum-dot high-β microcavities: transition from spontaneous emission to lasing and the effects of superradiant emitter coupling," Light: Sci. Appl. **6**, e17030 (2017).

Optics EXPRESS

13. E. Schlottmann, S. Holzinger, B. Lingnau, K. Lüdge, C. Schneider, M. Kamp, S. Höfling, J. Wolters, and S. Reitzenstein, "Injection locking of quantum-dot microlasers operating in the few-photon regime," Phys. Rev. Appl. **6**, 044023 (2016).
14. C. Redlich, B. Lingnau, S. Holzinger, E. Schlottmann, S. Kreinberg, C. Schneider, M. Kamp, S. Höfling, J. Wolters, S. Reitzenstein, and K. Lüdge, "Mode-switching induced super-thermal bunching in quantum-dot microlasers," New J. Phys. **18**, 063011 (2016).
15. M. Virte, K. Panajotov, H. Thienpont, and M. Sciamanna, "Deterministic polarization chaos from a laser diode," Nat. Photonics **7**, 1 (2012).
16. M. Marconi, J. Javaloyes, P. Hamel, F. Raineri, A. Levenson, and A. M. Yacomotti, "Far-from-equilibrium route to superthermal light in bimodal nanolasers," Phys. Rev. X **8**, 011013 (2018).
17. M. Soriano, J. García-Ojalvo, C. Mirasso, and I. Fischer, "Complex photonics: Dynamics and applications of delay-coupled semiconductors lasers," Rev. Mod. Phys. **85**, 421 (2013).
18. M. Sciamanna and K. A. Shore, "Physics and applications of laser diode chaos," Nat. Photonics **9**, 151 (2015).
19. A. Carmele, J. Kabuss, F. Schulze, S. Reitzenstein, and A. Knorr, "Single photon delayed feedback: A way to stabilize intrinsic quantum cavity electrodynamics," Phys. Rev. Lett. **110**, 013601 (2013).
20. S. M. Hein, F. Schulze, A. Carmele, and A. Knorr, "Optical feedback-enhanced photon entanglement from a biexciton cascade," Phys. Rev. Lett. **113**, 1 (2014).
21. F. Albert, C. Hopfmann, S. Reitzenstein, C. Schneider, S. Höfling, L. Worschech, M. Kamp, W. Kinzel, A. Forchel, and I. Kanter, "Observing chaos for quantum-dot microlasers with external feedback," Nat. Commun. **2**, 366 (2011).
22. C. Hopfmann, F. Albert, C. Schneider, S. Höfling, M. Kamp, A. Forchel, I. Kanter, and S. Reitzenstein, "Nonlinear emission characteristics of quantum-dot micropillar lasers in the presence of polarized optical feedback," New J. Phys. **15**, 025030 (2013).
23. P. Munnelly, B. Lingnau, M. M. Karow, T. Heindel, M. Kamp, S. Höfling, K. Lüdge, C. Schneider, and S. Reitzenstein, "On-chip optoelectronic feedback in a micropillar laser-detector assembly," Optica **4**, 303 (2017).
24. I. Reidler, Y. Aviad, M. Rosenblum, and I. Kanter, "Ultrahigh-speed random number generation based on a chaotic semiconductor laser," Phys. Rev. Lett. **103**, 024102 (2009).
25. X. Porte, M. C. Soriano, D. Brunner, and I. Fischer, "Bidirectional private key exchange using delay-coupled semiconductor lasers," Opt. Lett. **41**, 2871 (2016).
26. D. Brunner, M. C. Soriano, C. R. Mirasso, and I. Fischer, "Parallel photonic information processing at gigabyte per second data rates using transient states," Nat. Commun. **4**, 1364 (2013).
27. S. Reitzenstein, C. Hofmann, A. Gorbunov, M. Strauß, S. H. Kwon, C. Schneider, A. Löffler, S. Höfling, M. Kamp, and A. Forchel, "AlAs/GaAs micropillar cavities with quality factors exceeding 150.000," Appl. Phys. Lett. **90**, 251109 (2007).
28. C. Böckler, S. Reitzenstein, C. Kistner, R. Debusmann, A. Löffler, T. Kida, S. Höfling, A. Forchel, L. Grenouillet, J. Claudon, and J. M. Gérard, "Electrically driven high-q quantum dot-micropillar cavities," Appl. Phys. Lett. **92**, 091107 (2008).
29. S. Strauf, K. Hennessy, M. T. Rakher, Y.-S. Choi, A. Badolato, L. C. Andreani, E. L. Hu, P. M. Petroff, and D. Bouwmeester, "Self-tuned quantum dot gain in photonic crystal lasers," Phys. Rev. Lett. **96**, 127404 (2006).
30. S. M. Ulrich, C. Gies, S. Ates, J. Wiersig, S. Reitzenstein, C. Hofmann, A. Löffler, A. Forchel, F. Jahnke, and P. Michler, "Photon statistics of semiconductor microcavity lasers," Phys. Rev. Lett. **98**, 043906 (2007).
31. R. Hanbury Brown and R. Q. Twiss, "Correlation between photons in two coherent beams of light," Nature **49**, 27 (1956).
32. A. E. Lita, A. J. Miller, and S. W. Nam, "Counting near-infrared single-photons with 95% efficiency," Opt. Express **16**, 3032 (2008).
33. D. Drung, C. Assmann, J. Beyer, A. Kirste, M. Peters, F. Ruede, and T. Schurig, "Highly sensitive and easy-to-use SQUID sensors," IEEE Trans. Appl. Supercond. **17**, 699 (2007).
34. M. Schmidt, M. V. Helversen, M. López, F. Gericke, E. Schlottmann, T. Heindel, S. Kück, S. Reitzenstein, and J. Beyer, "Photon-number-resolving transition-edge sensors for the metrology of quantum light sources," J. Low Temp. Phys. (2018). https://doi.org/10.1007/s10909-018-1932-1.
35. J. Gérard, B. Sermage, B. Gayral, B. Legrand, E. Costard, and V. Thierry-Mieg, "Enhanced spontaneous emission by quantum boxes in a monolithic optical microcavity," Phys. Rev. Lett. **81**, 1110 (1998).
36. S. Reitzenstein, T. Heindel, C. Kistner, A. Rahimi-Iman, C. Schneider, S. Höfling, and A. Forchel, "Low threshold electrically pumped quantum dot-micropillar lasers," Appl. Phys. Lett. **93**, 061104 (2008).
37. C. J. Chang-Hasnain, J. P. Harbison, G. Hasnain, A. C. V. Lehmen, L. T. Florez, and N. G. Stoffel, "Dynamic, polarization, and transverse mode characteristics of vertical cavity surface emitting lasers," IEEE J. Quantum Electron. **27**, 1402 (1991).
38. R. Michalzik (ed.), *VCSELs: Fundamentals, Technology and Applications of Vertical-Cavity Surface-Emitting Lasers* (Springer-Verlag, 2013). https://doi.org/10.1007/978-3-642-24986-0.
39. P. Rice, and H. Carmichael, "Photon statistics of a cavity-QED laser: A comment on the laser phase-transition analogy," Phys. Rev. A **50**, 4318 (1994).
40. C. Gies, J. Wiersig, M. Lorke, and F. Jahnke, "Semiconductor model for quantum-dot-based microcavity lasers," Phys. Rev. A **75**, 013803 (2007).
41. E. Schöll, A. G. Balanov, N. B. Janson, and A. Neiman, "Controlling stochastic oscillations close to a Hopf bifurcation

Optics EXPRESS

by time-delayed feedback," Stoch. Dyn. **05**, 281 (2007).
42. E. Schlottmann, M. V. Helversen, M. Schmidt, M. López, F. Gericke, T. Heindel, S. Kück, S. Reitzenstein, and J. Beyer, "Exploring the photon-number distribution of bimodal microlasers with a transition edge sensor," Phys. Rev. Appl. **9**, 064030 (2018).
43. Z. Abdul Sattar, N. Ali Kamel, and K. A. Shore, "Optical injection effects in nanolasers," IEEE J. Quantum Electron. **52**, 1 (2016).
44. Y. D. Jeong, J. S. Cho, Y. H. Won, H. J. Lee, and H. Yoo, "All-optical flip-flop based on the bistability of injection locked Fabry-Perot laser diode." Opt. Express **14**, 4058 (2006).